Journal of
Materials Chemistry A

PAPER

View Article Online
View Journal | View Issue

Check for updates

Cite this: *J. Mater. Chem. A*, 2025, **13**, 36318

Probing photochemically-induced dynamic transitions by magic-angle-spinning NMR combined with *in situ* irradiation

Alessia Lasorsa,[a] Pieter van der Meulen,[b] Ernst Naumann,[c] Michael M. Lerch,[b] Rosa Marquez Garcia,[bd] Xiaohong Lan,[a] Katja Loos,[a] Ben L. Feringa,[b] Wiktor Szymanski[bd] and Patrick C. A. van der Wel*[a]

Light is often the stimulus of choice for dynamically changing structure and function in materials and other contexts, including not only many smart materials and photovoltaics, but also biological and biochemical processes. Proper understanding of the associated mechanisms requires insights into the underlying dynamic molecular and (photo)chemical transformations. Nuclear magnetic resonance (NMR) spectroscopy is a powerful tool for investigating these types of processes, providing unique chemical, structural, and dynamic information at the atomic level. Yet, while liquid-state NMR is increasingly regularly coupled with *in situ* irradiation, it is limited to soluble samples. Here we report on the application of *in situ* illumination to magic angle spinning (MAS) solid-state NMR (ssNMR). An *in situ* irradiation setup adapted to a customized MAS probe enabled sample illumination with high efficiency. We describe its technical features and illustrate its capabilities through representative case studies. These include photoresponsive azobenzene derivatives in solution and sequestered in hydrogels, a chemical actinometer in solution and UV-polymerization of vitrimer-like elastomers. We show how different ssNMR polarization transfer techniques can enable the study of dynamic transitions that accompany light-triggered (dis)assembly and cross-linking processes. We report on the efficient use of not only sapphire but also thin-wall zirconia rotors, in an approach compatible with the widely used Bruker-type MAS ssNMR instrumentation. We envision that these methods will enable diverse new research directions on photoresponsive materials, but also studies on photopharmacology, optogenetics, photocatalysis, and other light-driven systems.

Received 6th August 2025
Accepted 16th September 2025

DOI: 10.1039/d5ta06364g

rsc.li/materials-a

1. Introduction

Photochemical processes and applications are playing an increasingly important role in materials science, chemistry, as well as biochemical research. Noteworthy applications include lithography, molecular motors, UV curing, drug release and photopharmacology, photochromic applications, optogenetics, photocatalysis, and more.[1–7] These developments are accompanied by a need for spectroscopic approaches that probe mechanistic aspects, in terms of the chemical, structural and dynamic transitions. A wide range of spectroscopic techniques is in use, such as UV/vis, infrared (IR), electron paramagnetic resonance (EPR), and nuclear magnetic resonance (NMR) spectroscopy.[8–11] Among these, NMR offers the advantage of providing detailed structural information at the atomic and molecular levels, although it suffers from a lower temporal resolution and sensitivity. *In situ* irradiation NMR has become an attractive and accessible technique for analyses of compounds in solution.[8,12] It has been used for mechanistic and structural studies in photochemistry and photocatalysis.[13–22] However, many photochemical applications in materials science (and beyond) involve sample types that are unsuitable for liquid-state NMR due to high viscosity, rigidity or the presence of molecules with large molecular weights. Moreover, there is substantial interest in processes where irradiation is used to change the assembly state of samples, *e.g.*, triggering self-assembly or disrupting existing assemblies. In such cases, high order assemblies that lack rapid isotropic tumbling or flexibility disappear from liquid state NMR spectra, preventing the tracking of the full process. Modern magic angle spinning (MAS) solid-state NMR (ssNMR) has developed into a proven and powerful complement to liquid-state NMR, enabling the analysis of samples and materials that lack the fast isotropic

---

[a] *Zernike Institute for Advanced Materials, University of Groningen, Nijenborgh 3, 9747 AG Groningen, the Netherlands. E-mail: p.c.a.van.der.wel@rug.nl*

[b] *Stratingh Institute for Chemistry, University of Groningen, Nijenborgh 3, 9747 AG, Groningen, The Netherlands*

[c] *NAU-NMR TEC-CONSULT, Kreuzstraße 6, 76467 Bietigheim, Baden-Württemberg, Germany*

[d] *Department of Medicinal Chemistry, Photopharmacology and Imaging, Groningen Research Institute of Pharmacy, University of Groningen, Groningen, 9713 AV The Netherlands*

motion required for high-resolution liquid state NMR.[23] MAS NMR methods are applied not only to dry (powder) samples, but are applicable to semi-solids, soft matter, hydrogels, and solvated or hydrated sample conditions.[23,24] A crucial aspect is also that MAS NMR reveals not only chemical and structural transformations in atomic detail, but also changes in molecular motion that accompany (dis)assembly.[25,26] Thus, it would be a powerful tool to study photochemically driven chemical, dynamic and functional transformations. Yet, compared to liquid state NMR, its use in photochemical applications has been more limited.

Some technical features of MAS NMR are relevant to understanding challenges to its use in photochemical research. First, normal MAS NMR sample holders are not very transparent, limiting convenient sample irradiation (*in situ* or *ex situ*). During NMR, the sample holders ('rotors') need to be rotated at thousands of times per second within the coil used for radio frequency (RF) pulsing and detection.[27] These rotors are typically manufactured from zirconia (Fig. 1A and B) and machined to high precision, to enable stable rotation and withstand the associated mechanical stress. Zirconia rotors are opaque to UV and visible light (Fig. 1B). Sapphire rotors have improved optical transparency (Fig. 1B), but have more limited safe spinning rates.[28–31] Sapphire rotors are nowadays commercially available, driven by their use in dynamic nuclear polarization (DNP) experiments requiring microwave irradiation *in situ*.[29,32–34] So, these transparent rotors address one concern. However, a second issue is that *ex situ* irradiation is only of limited use, even if it can be conveniently done with transparent rotors. The process of transferring an irradiated sample into the NMR probe, and getting it prepared for NMR measurements, would exceed 5 minutes at minimum. This makes *ex situ* irradiation less useful (or even ineffective) for short-lived states, intermediates, and out-of-equilibrium conditions. Under such conditions, which are of significant interest and importance, *in situ* irradiation is essential.

Generally speaking, there are two approaches to performing *in situ* irradiation in MAS NMR: longitudinal (or axial) and transverse irradiation. In the former case, one attempts to irradiate the sample by sending light along the long axis of the rotor, while the latter involves irradiating through the side walls of the rotor. Recent studies have advocated for the longitudinal irradiation approach, based on its convenience in implementation.[35–37] Longitudinal irradiation approaches so far rely on the use of rotors with a so-called 'pencil' design. In this MAS rotor design, the top-cap is exposed during MAS and can therefore relatively easily be modified and accessed (Fig. S1). Thus, it can be replaced with a tapered glass rod to allow transmission of the light into the rotor. This approach is suitable for pencil rotors, but it is not easily adapted to the more widely used Bruker type MAS rotors that lack an exposed end cap. Moreover, as discussed below, the irradiation efficiency is reduced by the long pathlength.

Here we describe our approach to *in situ* irradiation applicable to the more common Bruker-style rotors. We rely on transverse irradiation, where light is delivered to the side of the MAS rotors (between the windings of the RF coil), using a light-fiber installed into the body of the probe. The advantage of this approach is that the sample rotation provides a natural means of uniform sample irradiation. Moreover, the pathlength for light delivered into the sample is relatively short, and much shorter than during longitudinal irradiation. Our approach combines features from previously reported *in situ* illuminated MAS NMR, a field that goes back many years. However, most of the prior work was focused on biochemical applications, especially light-responsive proteins, in contrast to the applications reported below.[28,30,31,37–52] Another important feature of our work is the use of (affordable) LED (light emitting diode) light sources

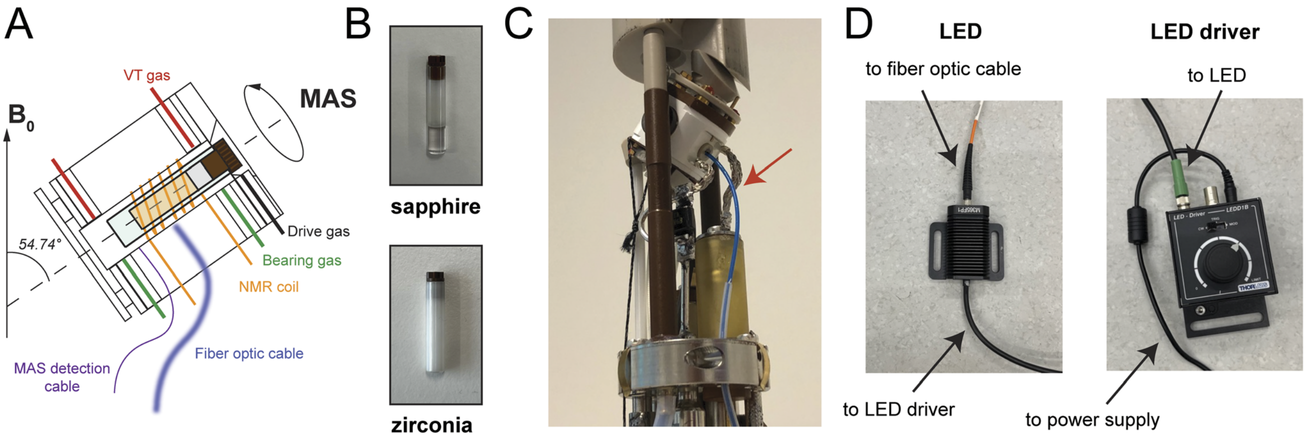

Fig. 1 Instrumentation and MAS NMR probe modifications for *in situ* illumination. (A) Schematic of the transverse illumination setup in context of the Bruker-style MAS NMR stator design. Pathways for the typical drive and bearing gas that enable the MAS are indicated. The MAS rotor is shown with its drive cap with fins at the top, near the drive gas entry point. The fiber optic cable approaches the rotor from the side, with the light passing between the windings of the metal RF coil. (B) Photographs of zirconia and sapphire MAS rotors for the Bruker-style stator. Shown are rotors with a 3.2 mm outer diameter, and internal volumes in the range of 30–50 μL. (C) Photo of the installed NMR coil with penetrated optic fiber. The fiber optic cable that enters a hole in the coil holder at the bottom of the stator is indicated by the red arrow. (D) Photos of the other end of the light fiber, mated to the LED-based light source, and its adjustable LED driver.

that are nowadays common in photochemical research.[35,36,51–54] Classic MAS NMR studies relied heavily on high-power light sources (Xe lamps and lasers), which meant that the efficiency of irradiation delivery was less critical. The use of LED sources requires a closer focus on evaluating irradiation efficiency. Thus, we applied our setup to several relevant photochemical systems, including an actinometer,[55] in order to evaluate illumination efficiency. We observe highly efficient illumination, enabling faster photochemical control than previously described by longitudinal irradiation. We discuss a number of technical aspects related to *e.g.*, interference with the standard light-based MAS detection, and the comparison of sapphire and zirconia rotors. We demonstrate how this *in situ* illumination approach can be combined with ssNMR analyses of sample dynamics relevant to the photochemical and materials science community. We tested applications on photoswitchable molecules in semi-solid materials (hydrogels) and UV-hardening polymer matrices, illustrating the potential of these types of approaches and instrumentation.

2. Results and discussion

2.1 Description of the *in situ* irradiation solid-state NMR setup

We set out to implement *in situ* irradiation in context of a Bruker-type MAS probe for use with 3.2 mm MAS rotors. A Bruker MAS NMR probe was modified to allow transverse irradiation of the rotor, for use with transparent (sapphire) rotors available for DNP applications. Holes in the probe body allowed a fiber optic cable to be guided from the bottom of the probe into the stator (Fig. 1C). The fiber optic cable can be connected to different LED sources, with a sufficiently long fiber to permit some distance between the ultra-shielded NMR magnet and LED (Fig. 1D). The illumination intensity can be modulated using an LED driver. A fiber optic cable with optimal transparency for wavelength range 400–2200 nm was used. The stator base contains the typical cuboidal coil holder, made from boron nitride, that holds the solenoid NMR coil. This coil holder was outfitted with a central borehole to permit entry of the fiber close to the sample. A challenge is that the light has to penetrate the RF coil within the stator.[27] For many standard coil designs, one would expect a partial blocking of the light by default closely-spaced coil windings. To address this concern, a pitched coil was used with non-uniform distances between the windings, enabling a larger opening between the windings near the sample center and avoiding coil wire directly above the borehole of the holder (Fig. 1A). The light fiber was placed such that the fiber end was at an estimated distance of 1–2 mm from the rotor sleeve surface.

The probe was designed and intended for use with sapphire (transparent) rotors. In initial tests, we observed effective irradiation of the sample, but also interference between the irradiation light and the optical MAS rate detection system. The latter is based on the shining of light (wavelength near 650 nm) on or near the bottom end of the rotor, with the MAS rate inferred from changes in reflected light due to markings on the rotor. Light leakage was found to disrupt this detection and prevent reliable MAS operation. To overcome this issue, we modified the MAS detection fiber optic cable with an added band-pass filter at 650 nm. This filter prevents interference from the irradiation light with MAS detection, based on differences in the employed wavelengths. This implies that this specific range (650 ± 10 nm) is not available for *in situ* irradiation, at least not without further changes. In our tests, this configuration allows stable and reliable MAS, in presence and absence of irradiation.

2.2 MAS NMR of a chemical actinometer to evaluate the efficiency of light delivery

Next, we performed test and validation experiments with light-responsive materials and samples, first focusing on the analysis of the efficiency of light delivery to the sample. The compound *ortho*-nitrobenzaldehyde (*o*-NBA) is a well-known chemical actinometer that under irradiation isomerizes to *ortho*-nitrosobenzoic acid with a quantum yield of 0.5 and an absorption spectral range of 300–410 nm.[55] *In situ* LED liquid-state NMR has already been utilized for meticulous quantum yield determination of *o*-NBA.[56] In this approach, initial photochemical conversion from *o*-NBA to *o*-nitrosobenzoic acid under UV light ($\lambda = 365$ nm) can be measured to assess the efficiency of sample irradiation. A 15 mM solution of *o*-NBA was prepared in DCM-d_2. A sapphire 3.2 mm rotor was loaded with 20 μL of this solution, and the rotor was sealed with a Teflon spacer between the sample and the rotor cap. This sample was subjected to *in situ* irradiation at $\lambda = 365$ nm while spinning at 3.5 kHz MAS. Fig. 2A shows photographs of the rotor before and after (*in situ*) irradiation. Upon irradiation, the solution turns yellow due to the reactivity of the nitroso group, which can undergo self-reaction to form azobenzene-type compounds. The same figure includes NMR spectra recorded during the first 10 minutes of exposure. In the initial spectrum, before irradiation, a signal from the solvent DCM can be observed at 5.4 ppm, along with several signals from *o*-NBA. A distinct signal at 10.5 ppm corresponds to the aldehyde group, and three additional signals between 7.8 and 8.3 ppm correspond to the four aromatic protons. Upon irradiation, new signals appear at 6.6, 7.8, 8.1, and 8.5 ppm, marked with stars, indicating the formation of the product. These signals, which have similar integral values, correspond to the four aromatic protons of the *o*-nitrosobenzoic acid product. The peak at 10.5 ppm, attributed to the aldehydic proton of *o*-NBA, and the peak at 6.6 ppm, corresponding to the photoconversion product, are used to determine the initial reaction rate (Fig. 2B). In a relatively small time interval and at the beginning of the reaction, the conversion rate can be approximated by a linear equation. Thus, time points in the first 7 minutes were used to obtain an estimate of the initial rate. Based on the decrease in reactant concentration, the estimated initial rate is equal to -1.05 mM min^{-1} (Fig. 2C). A similar value is obtained by evaluating the formation of the reaction product (Fig. S2). This value is of the same order of magnitude as the previously reported value of 0.368 mM min^{-1} (where the authors used an initial concentration of 13 mM).[56] The extracted rate can be used to obtain an estimate of the light

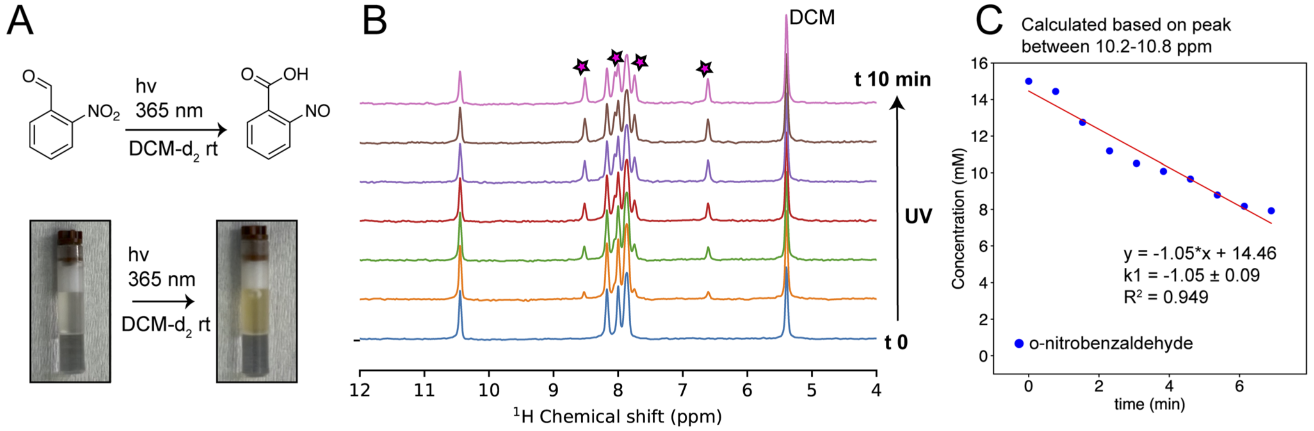

Fig. 2 *In situ* illumination and MAS NMR of a chemical actinometer. (A) Photochemical transformation of *o*-nitrobenzaldehyde to *o*-nitrosobenzoic acid at $\lambda = 365$ nm (top). Photo of the rotor before and after *in situ* irradiation (for 16 min). (B) ^{1}H MAS NMR spectra recorded under continuous irradiation during the first 10 minutes of the reaction. Peaks corresponding to the reaction product are marked with stars. The solvent peak is marked with DCM. (C) Plot of peak intensity between 6 and 7 ppm as a function of the illumination time. The solid line is a linear fit to the data, with fit parameter shown in the inset. Experiments were conducted at a MAS spinning rate of 3.5 kHz and a temperature of 290 K under continuous irradiation at 365 nm.

intensity reaching the sample (I_0), using the following equation:[55]

$$-\frac{\mathrm{d}[o\text{-NBA}]}{\mathrm{d}t} = I_0\Phi\left(1 - 10^{-\varepsilon b[o\text{-NBA}]}\right)$$

where the term at the left is the estimated rate (−1.05 mM min^{-1}), Φ is the quantum yield of the compound (*i.e.*, 0.5), ε is the molecular absorptivity (*i.e.*, 265 M^{-1} cm^{-1}) and b is the path length (~1.1 mm, half of the rotor inner diameter). With all other variables known, the light intensity can be determined as equal to 55.2 µeinstein L^{-1} s^{-1} (*vs.* 24.3 µeinstein L^{-1} s^{-1} reported in the prior study). Consistently, product decomposition was also observed (already after 15 minutes of irradiation). Based on these rates and light intensity estimates, our setup is capable of similar irradiation efficiencies as *in situ* illumination liquid state NMR, despite the more demanding technical implementation as described above.

2.3 Application to azobenzene photoswitches in aqueous solution

As another test that permits comparison to alternative approaches, *in situ* irradiation MAS NMR was performed on an aqueous solution of a water-soluble azobenzene-derivative. Azobenzene molecules are widely used in photochemical studies due to their ability to reversibly switch between *cis*/*trans* configurations upon irradiation at specific wavelengths.[1,57] A common challenge with azobenzenes is their low solubility under aqueous conditions, leading to rapid aggregation.[58] The azobenzene derivative ((*E*)-(4-((4-methoxyphenyl)diazenyl)phenyl)methanamine 2,2,2-trifluoroacetate) was synthesized as described in the SI, featuring an ammonium group to enhance water solubility and a methoxy group to increase the photostationary state distributions (Fig. 3A). The compound was dissolved in D_2O at a concentration of 2.5 mg mL^{-1} (~7 mM) as a sample for MAS NMR studies. 20 µL of this solution was inserted into a sapphire rotor, as above. The sample was irradiated with UV light at 365 nm (Fig. 3A) and the real-time *trans*-to-*cis* isomerization of the molecule was monitored by acquiring ^{1}H NMR spectra (Fig. 3B). The *trans* and *cis* isomers of azobenzene exhibit distinct ^{1}H NMR signals, allowing their interconversion to be easily monitored by NMR. Before irradiation, the initially observed spectrum predominantly shows peaks consistent with the *trans* configuration, with around 10% of the signal attributable to the *cis* isomer, based on peak integration. The thermodynamically stable *trans* form displays characteristic signals at 3.9 ppm and 4.3 ppm, corresponding to the methoxy and methylene groups, respectively. Aromatic protons appear at 7.2, 7.6, 7.8, and 7.9 ppm. In the *cis* form, all peaks shift to different chemical shift values. The methoxy and methylene groups appear at 3.8 ppm and 4.1 ppm, while the aromatic protons are observed at 6.9, 7.0, and 7.4 ppm. Upon illumination, the signals from *trans* diminished and the *cis*-form signals increased following typical first order kinetics, until complete conversion after less than 12 minutes. The reaction was studied at room temperature with and without MAS rotation (at 0 and 4 kHz MAS) (Fig. 3C). The effect of MAS on irradiation efficiency was assessed by plotting the intensity of representative *cis* and *trans* peaks as a function of time: the overlapping trans peaks at 7.8 and 7.9 ppm, and the *cis* peak at 7.0 ppm. The *trans* peak shows a slightly faster decay at 4 kHz MAS compared to the static mode; however, the observed difference is relatively small (less than 10%), as may be expected for a liquid sample.

2.4 Effective sample irradiation in different rotor materials

To test the effect of the rotor wall material, the same irradiation experiment on the azobenzene sample was performed with both sapphire and thin wall zirconia rotors. The latter rotors are most commonly used for MAS NMR, but are largely opaque (Fig. 1B). Fig. 4 shows that use of the sapphire rotor gives faster

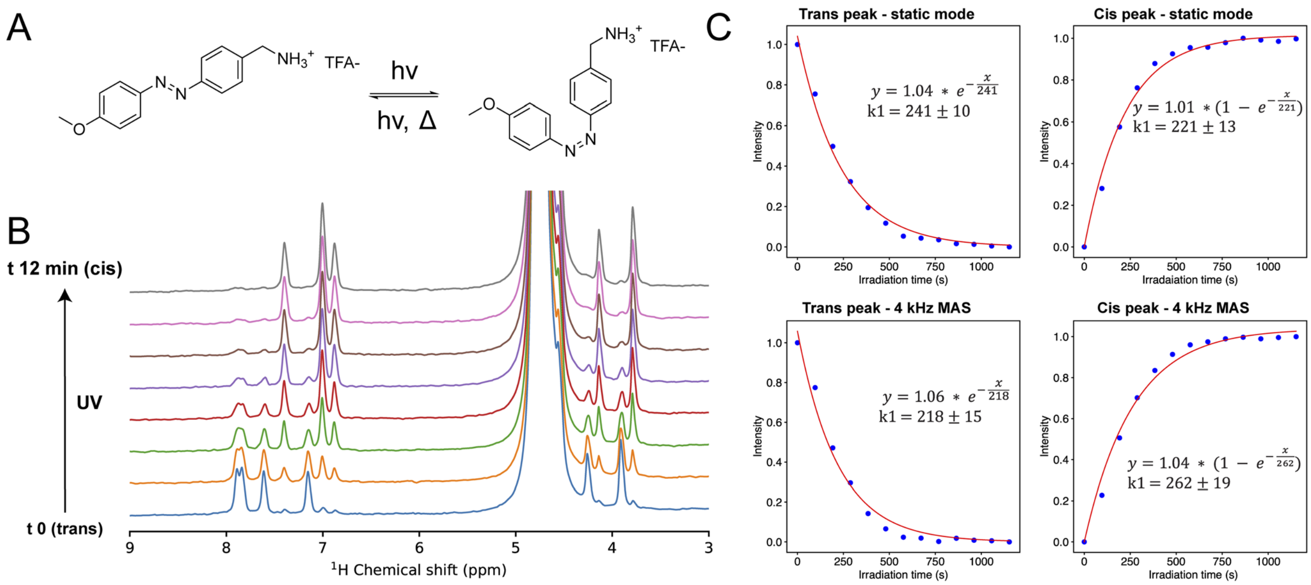

Fig. 3 *In situ* irradiation MAS NMR of a water-soluble azobenzene derivative. (A) *Trans*-to-*cis* conversion of dissolved azobenzene mediated by UV light at 365 nm. (B) ^{1}H MAS NMR spectra recorded during the first 12 minutes of the *trans*-to-*cis* conversion under continuous irradiation at 365 nm and 4 kHz MAS. (C) Experimental and fitted plot of the *trans* (between 7.7 and 8.0 ppm) and *cis* (between 6.9 and 7.1 ppm) peak intensity *versus* the reaction time at 4 kHz MAS and in static mode. Experiments were conducted at a constant temperature of 298 K, and under continuous irradiation at 365 nm.

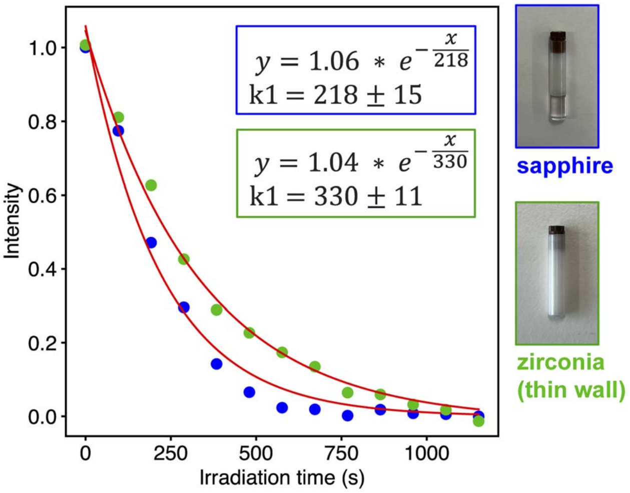

Fig. 4 Photochemical transformation kinetics in zirconia rotors. Relative peak intensity of the *trans*-azobenzene in solution as a function of irradiation time. Blue dots represent experimental data for sapphire rotor and green dots for a thin-wall zirconia rotor. See also photos of example rotors. Peak intensities were integrated from ^{1}H chemical shifts between 7.7 and 8.0 ppm. The solid lines represent fits to the experimental data, using the formulas shown in the inset. Experiments were conducted at a MAS spinning rate of 4 kHz, a temperature of 298 K, and under continuous irradiation at 365 nm.

transformation kinetics (blue dots), as expected. However, even in the zirconia rotor, substantial switching was observed, showing that the light transmission efficiency through the thin wall rotor is surprisingly good, and likely sufficient for many applications. This is a relevant point, as such rotors are more commonly available, easier to spin (to a higher MAS rate), and can accommodate more sample volume.

Thus, both the actinometer analysis on *o*-NBA and the analysis of dissolved azobenzene point to a highly efficient sample irradiation in our setup, which is compatible with the widely used Bruker-type MAS rotors. Indeed, even traditional zirconia rotors seem usable in such studies, although the degree of transparency is expected to be wavelength dependent (with worse performance below 300 nm). A recent study[35] reported on a similar azobenzene experiment, using the end-on irradiation approach discussed in the Introduction. In that study, the conversion took about 4 hours, compared to 12 minutes in our setup. Although various details were different (solvent, azobenzene structure, concentration), we assume that a key difference relates primarily to the efficiency of light transmission. For instance, the pathlength in our samples illuminated from the side should be significantly shorter than when performing longitudinal end-on irradiation of pencil rotors.[35,36,52]

2.5 MAS NMR of azobenzene sequestered in an alginate hydrogel

MAS NMR is an essential tool for applications involving solid and semi-solid samples, based on its ability to dissect the chemical structure, molecular motion, and interactions *via* a diverse toolkit of NMR experiments.[23,25,59] Next, we tested our setup on a semi-solid (yet transparent) material, as we incorporated the same azobenzene into an alginic acid-based hydrogel. Alginic acid is widely used to make hydrogels, *e.g.*, by cross-linking with divalent Ca ions, such that guest molecules can be encapsulated.[60,61] Here, alginic acid (medium viscosity) was dissolved in a D_2O solution of azobenzene (2.5 mg mL^{-1}, ∼7 mM). To cross-link the alginate, $CaCl_2$ solution was added, yielding a hydrogel that was yellow in color. Next, a zirconia thin-wall rotor was packed with 34 mg of the azobenzene-containing hydrogel (Fig. 5A). Fig. 5B presents the ^{1}H MAS NMR spectra recorded both before and during illumination at increasing time intervals. Notably, in the initial ^{1}H spectrum (blue), no azobenzene peaks are distinguishable (compare to Fig. 3). The spectral region above 6 ppm is empty, while the region with lower chemical shifts (between 4.5 and 3.5 ppm) is dominated by alginate protons. The lack of detectable azobenzene signal shows that the azobenzene is immobilized in the hydrogel. As shown in Fig. 3, dissolved azobenzene molecules produce narrow ^{1}H peaks (*i.e.*, have relatively long ^{1}H T_2 times). Immobilization results in peak broadening due to a shortening of the T_2 and increased manifestation of anisotropic interactions, to such an extent that the peaks become essentially invisible in the spectrum.[25] Interestingly, upon irradiation, aromatic peaks corresponding to the *cis* form of azobenzene become visible (Fig. 5). These peaks increase in intensity until 16 minutes of irradiation, after which the conversion reaches a plateau. The appearance of the signals upon switching are attributed to the disruption of immobilizing interactions upon *trans* to *cis* interconversion. Further insights were gained by synthesizing a ^{13}C-labeled version of the same compound (^{13}C-methoxy azobenzene). This selective labeling enabled the acquisition of ^{13}C NMR spectra using various polarization transfer techniques, including ^{1}H-^{13}C CP (cross-polarization), ^{1}H-^{13}C INEPT (insensitive nuclei enhanced by polarization transfer), and ^{13}C direct excitation (DE). Each of these techniques has a different sensitivity to molecular dynamics, enabling the convenient detection of dynamic transitions.[25,59,62] The full spectra are shown in Fig. S3, while the methoxy region of the CP and INEPT spectra is highlighted in Fig. 5D. In absence of irradiation, we observe a visible peak of the labeled methoxy group in the CP spectrum (bottom; solid line), but upon irradiation, this CP signal disappears. The CP experiment only works for immobilized or rigid molecules and gives no signals for dissolved and highly mobile species.[25] Thus, we can observe the light-induced mobilization of the azobenzene in these ^{13}C NMR measurements. This conclusion is supported by complementary INEPT experiments, which highlight mobile molecules: the obtained signal is highly dependent on the transverse relaxation (T_2) of ^{1}H and ^{13}C nuclei such that only highly flexible or rapidly tumbling molecules are detected, and immobilized molecules are invisible. Upon irradiation, the ^{13}C INEPT signal of the methoxy group increases (Fig. 5D top), showing an increase in dynamics. The low intensity of the CP signal (above) and the presence of a modest INEPT peak (in absence of irradiation) indicate that the *trans* isomer of the azobenzene is only partly immobilized in this hydrogel. This may be due to a dynamic equilibrium between an immobilized and mobile state. The observed azobenzene immobilization could be due to aggregation of the compound (possibly induced

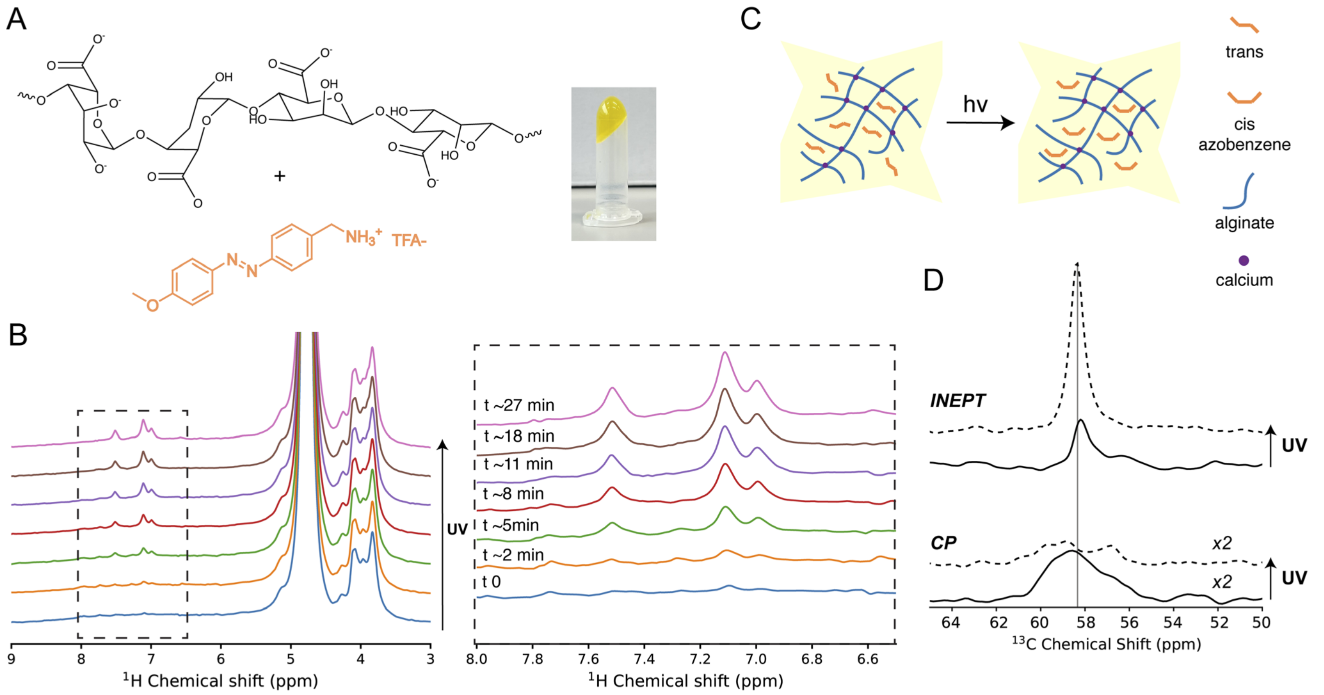

Fig. 5 ^{1}H MAS NMR of azobenzene-containing hydrogels. (A) Chemical structures of alginic acid and the used azobenzene, and photograph of the azobenzene-containing hydrogel. (B) ^{1}H MAS NMR spectra obtained under continuous irradiation. The spectra stopped changing after about 16 min. The right spectra show a zoomed-in region, showing signals of the *trans* azobenzene. (C) Schematic of the *trans*-to-*cis* conversion of the azobenzene occurring in the hydrogel. (D) Methoxy region of ^{13}C MAS ssNMR spectra of methoxy-^{13}C azobenzene-containing hydrogel recorded using INEPT and CP, before (solid black line) and after (dashed black line) irradiation. The experiments were conducted at a MAS spinning rate of 12 kHz, a constant temperature of 298 K, and continuous irradiation at 365 nm.

by π–π stacking), interactions with the hydrogel matrix, or a combination of effects. This case study is an illustrative example of the potential for deploying *in situ* irradiated MAS NMR for studying dynamic aspects of photoresponsive materials and hydrogels, for delivery of drugs and in other contexts.[63,64]

2.6 *In situ* MAS NMR of a light-mediated radical polymerization reaction

Another interesting application of photochemistry is in processes where materials are being cross-linked or otherwise modified by (*in situ*) irradiation. In a recent paper, some of us presented a sustainable approach for creating vitrimer-like elastomers based on lipoic acid, a naturally occurring compound capable of forming dynamic disulfide bonds.[65] Through a combination of ring-opening polymerization, post-functionalization, and UV-induced crosslinking, a series of elastic, recyclable, and self-healing materials were developed without the use of initiators or catalysts. These lipoic acid-based vitrimer elastomers (LAVEs) exhibit low hysteresis, high thermal stability, and tunable mechanical properties, making them highly promising for use in soft robotics, wearables, and other applications requiring long-term mechanical integrity and adaptability. Understanding the kinetics and mechanism of the UV-triggered crosslinking process is key for optimizing material design, curing conditions, and ultimately tailoring functionality for specific applications. We packed starting material "EG-CV-10-LA" (Fig. 6A) into a sapphire MAS rotor and then performed *in situ* irradiation at $\lambda = 365$ nm and 10 kHz MAS. Spectra were measured following *in situ* irradiation for different time periods. ^{1}H 1D and ^{13}C 1D spectra were acquired, with representative spectra reported in Fig. 6B and C. The ^{13}C spectra were again measured using different polarization transfer techniques to observe changes in molecular dynamics, this time as a consequence of the polymerization process.[25,62] The ^{1}H-decoupled ^{13}C DE experiment provides signal intensities that are semi-quantitative: *i.e.*, the peak intensity is a good indicator of the relative amounts of detected chemical groups or compounds. As discussed above, ^{13}C signals obtained *via* CP or INEPT experiments are modulated by dynamics,[25,62] and can thus be used to track polymerization due to UV illumination.

Fig. 6B shows ^{1}H MAS NMR spectra before and after *in situ* irradiation (for 24 h). The change in polymerization state can be observed by spectral changes, associated with the UV-induced ring opening (marked 'h' in panels A and B). Fig. 6C shows in purple the ^{13}C-detected INEPT, DE and CP spectra for the sample prior to irradiation, displayed with comparable vertical scaling. Strong and narrow peaks are seen by INEPT and DE, whilst the CP spectrum is much weaker, as expected for the non-polymerized starting material. Peak assignments are discussed in Fig. S2. Upon irradiation, several peaks in the DE spectrum decrease in intensity and even disappear, indicating a chemical transformation due to the crosslinking. Moreover, the INEPT spectrum shows a decreased intensity for several additional peaks, due to changes in (sample) mobility (zoom in Fig. 6D). As the monomers are linked, they become increasingly rigid, leading to a shortening of the T_2 and a decreased INEPT polarization transfer efficiency. The CP spectrum instead shows increasing peak intensities, consistent with the rigidification of (parts of) the sample (see also Fig. S4). In the INEPT spectra, most signals show a gradual reduction in intensity without chemical shift changes, while the peaks corresponding to the carbons labeled as g, i, and h in the chemical structure (1,2-dithiolane ring) disappear after just 2 hours of irradiation. Thus, the NMR-detected progression of these chemical and dynamic transitions can be visualized based on the chemical shift changes and intensity changes of the distinct peaks over time (Fig. S4D). The 1D spectra shed light on changes in the sample chemical structure and sample mobility, but are limited in their resolution and molecular detail. In addition to the time-dependent 1D spectra, 2D ^{1}H–^{13}C HETCOR spectra were also acquired before and after irradiation (Fig. 6E). These spectra allow for deeper analysis of the observed signals and support the interpretation of the 1D peak assignments. In this type of spectrum, each peak reflects a H–C chemical bond. Comparing the before- and after-irradiation spectra, we have marked disappearing peaks for the carbons directly affected by the ring-opening reaction (labeled with g, h, i). A caveat of these types of 2D spectra is that they take considerable time to acquire (typically hours). As such, they are most effective for gradual or irreversible processes (as shown here), for dynamic equilibria, or when combined with time-resolved 1D spectroscopy.

2.7 Perspectives on technical enhancements and future developments

The above examples highlight the ability of suitably implemented modern MAS ssNMR to identify and study not only chemical transformations, but also dynamic changes (*e.g.*, due to self-assembly) upon sample irradiation. We observed the applicability to semi-solid sample conditions, where liquid state NMR is impractical or impossible, and showed how we could monitor several types of transformations. The applications in this study are primarily designed to illustrate the principles and capabilities of this method, and to pave the way for wider adoption in the field. The illustrated NMR methods provide insights into chemical, conformational, and dynamic changes, complementing insights from other spectroscopic methods such as EPR or vibrational spectroscopy, which can offer greater sensitivity and better time resolution. The combined use of widely available Bruker MAS NMR equipment, LED light sources and potentially even zirconia rotors may facilitate a cost effective and versatile approach accessible to more groups in the community. The presented approach is complementary to recent reports of 3D printed devices designed for longitudinal irradiation, which is primarily suitable for the alternative 'pencil' rotor designs. As noted, our data suggest more effective irradiation in our setup, likely due to the reduced pathlength and beneficial effects of sample rotation during transverse irradiation. Naturally, further improvements may be envisioned. The zirconia rotors were found to be surprisingly usable, but still suffered from reduced light penetration. Literature on zirconia absorbance suggests that transmission losses

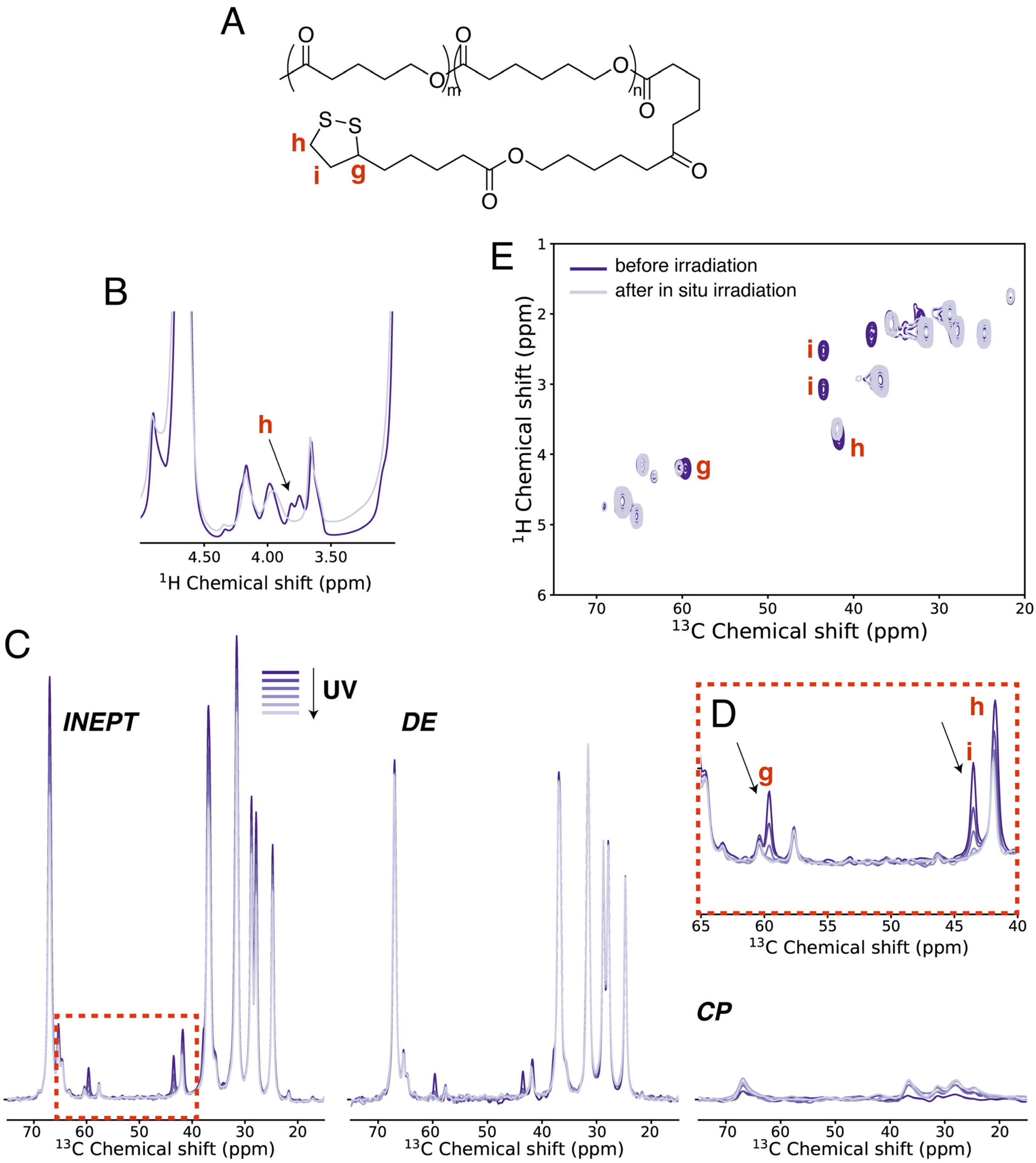

Fig. 6 UV-induced photo-crosslinking. (A) Chemical structure of EG-CV-10-LA, with the carbon atoms of the 1,2-dithiolane ring labeled as g, i, and h. (B) ^{1}H MAS NMR spectra of the material before and after irradiation, showing the disappearance of the 'h' protons. (C) ^{13}C MAS NMR spectra recorded using different polarization transfer techniques: INEPT, DE, and CP. Time points are 0 h (dark purple), ~1 h, ~2 h, ~5 h, ~10 h, and ~24 h (light purple). (D) Zoomed region from the INEPT spectrum in (C) highlighting the disappearance of at least two peaks (indicated by arrows) as a function of irradiation time. (E) ^{13}C–^{1}H INEPT HETCOR spectra recorded before and after irradiation, highlighting peaks belonging to the 1,2-dithiolane ring that disappear due to polymerization. All experiments were performed at a MAS spinning rate of 10 kHz, a temperature of 298 K, and continuous irradiation at 365 nm.

for this rotor material become most substantial below 365 nm,[66] such that the usability is likely dependent on the wavelengths needed. Sapphire rotors still offer real benefits in this area, while alternative rotor materials such as diamond[67] may also be advantageous. Other potentially useful extensions could involve the combination with polarization enhancement techniques, which could be valuable or even essential for ensuring sufficiently short acquisition times to permit good time resolution in the NMR experiments. Techniques such as the already mentioned DNP and in particular photochemically induced

DNP (photo-CIDNP) would be interesting complements, which are undergoing continuing development in the literature.[31,68–70] Another useful extension could involve the application to smaller rotor sizes that could maximize sample penetration as well as sensitivity (*e.g.*, ^{1}H detection), but also offers technical challenges for its practical implication.

3. Conclusions

We reported here photochemical applications of an *in situ* irradiation setup in a customized 3.2 mm Bruker NMR MAS probe. We have shown that this setup enables transverse sample irradiation in sapphire rotors, but also in thin-wall zirconia rotors. We found that our setup yielded a high irradiation efficiency, that was comparable to liquid-state NMR reports where light fibers are placed into samples. Our findings show that transverse illumination has advantages that may outweigh those of longitudinal irradiation setups. One practical point is that many research groups and NMR facilities have MAS NMR probes using the Bruker rotor design, which is not easily compatible with the latter. We presented case studies that illustrate the combination with dynamically sensitive MAS NMR experiments, including photoswitch-containing hydrogels and UV-induced polymerization reactions. A crucial point is that we observed not only chemical changes, but also the elucidation of dynamic changes in irradiated samples. We believe that these MAS NMR approaches will prove to be valuable tools for studying light-induced self-assembly and disassembly processes that are difficult or impossible to observe by other spectroscopic techniques. Thus, modern *in situ* illuminated MAS NMR can serve as an essential tool for a range of research fields including photochemical studies, photocatalysis, materials science applications, as well as biophysical, photopharmacological, biochemical and optogenetics applications.

4. Methods

4.1 Solid-state NMR

Solid-state MAS NMR spectra were recorded on a Bruker AVANCE NEO 600 MHz (14.1T) spectrometer equipped with a 3.2 mm BB/HX MAS probe modified for *in situ* irradiation, as described in the Results section. A fiber optic cable with a coating diameter of 1040 μm and a core diameter of 600 μm was used, with optimal transparency for wavelength range 400–2200 nm (part number FT600EMT, from Thorlabs). The LED source and driver were M365FP1 – 365 nm and T-Cube™ LED Driver – LEDD1B, both from Thorlabs. Samples were packed into either 3.2 mm transparent sapphire or 3.2 mm thin wall zirconia rotors using a PTFE top-insert spacer. The MAS and temperature setpoint are indicated in each figure caption. ^{1}H and ^{13}C chemical shifts were referenced to aqueous DSS, using the indirect method, by measuring the adamantane ^{13}C signals and by setting the high-frequency adamantane peak to 40.49 ppm.[71] Spectra were acquired with Bruker Topspin software, processed using NMRPipe and visualized with Python code adapted from the resources available in nmrglue.[72,73] Peak integration and data fitting were also performed with Python. Additional experimental parameters are reported in Table S1.

The 2-nitrobenzaldehyde (*o*-NBA; purchased from Merck, Cat. No. N10802) was dissolved in DCM-d$_2$ at a concentration of 15 mM. 20 μL of this solution was loaded into a sapphire 3.2 mm rotor. A Teflon spacer was then placed between the sample and the rotor cap. Here, ^{1}H (600.13 MHz) MAS NMR spectra were acquired using the "one pulse" program with a ^{1}H 90° pulse of 3 μs (rf strength: 83 kHz), a recycle delay of 10 s and 4 scans. Continuous irradiation at 365 nm (current limit on the LED driver was set to 1.0 A) was performed for a total of 16 minutes, and spectra recorded in the first 10 minutes were used for data fitting.

The azobenzene-containing samples were prepared as described below. ^{1}H (600.13 MHz) MAS NMR spectra of dissolved azobenzene were acquired using the "one pulse" program with a ^{1}H 90° pulse of 3 μs (rf strength: 83 kHz), a recycle delay of 4 s and 16 scans. Continuous irradiation was performed at 365 nm with current limit on the LED driver set to 1.0 A. ^{13}C MAS NMR rotor-synchronized refocused insensitive nuclei-enhanced polarization transfer (rINEPT), cross-polarization (CP) and direct excitation (DE) experiments used 50 kHz ^{13}C nutation frequency (5 μs 90° pulse), 4 s recycle delay, and 4k scans. During acquisition, 71.4 kHz two-pulse phase modulation (TPPM) ^{1}H decoupling was applied in all experiments.[74] For the 1D ^{13}C CP, a 70–100% ramped ^{1}H–^{13}C CP step was used, with contact time set to 1500 μs.

The polymer sample (EG-CV-10-LA) was packed into a sapphire 3.2 mm rotor with a Teflon spacer placed between the sample and the cap. Here, ^{1}H (600.13 MHz) MAS NMR spectra were acquired using the "one pulse" program with a ^{1}H 90° pulse of 2.5 μs (rf strength: 100 kHz), a recycle delay of 4 s and 128 scans. ^{13}C MAS NMR rINEPT and DE experiments used the following parameters: 50 kHz ^{13}C nutation frequency (5 μs 90° pulse), 0.022 s acquisition time, 3.5 s recycle delay, and 256 scans; 1D ^{13}C CP used instead 0.015 s acquisition time, while other parameters were kept the same. During acquisition, 71.4 kHz TPPM ^{1}H decoupling was applied in all experiments.[74] For the 1D ^{13}C CP, a 70–100% ramped ^{1}H–^{13}C CP step was used, with contact time set to 1000 μs. 2D INEPT-based HETCOR spectra were recorded using ^{13}C nutation frequency of 50 kHz, ^{1}H nutation frequency of 83 kHz, 3 s recycle delay, and 32 scans per data point, in absence of homonuclear decoupling during the t1 evolution. TPPM ^{1}H decoupling during acquisition was set around 71.4 kHz. Continuous irradiation was performed at 365 nm with current limit on the LED driver set to 1.0 A.

4.2 Azobenzene and alginate hydrogel NMR sample preparation

The azobenzene (or the ^{13}C-methoxy azobenzene) compound (see below) was dissolved in D$_2$O at a concentration of 2.5 mg mL^{-1} (~7 mM). This solution was first filtered (Fisherbrand™ Syringe Filter PES, 0.45 μm), to remove residual particulates. Of this stock solution, 20 μL was used to pack either a transparent sapphire rotor (provided with a top spacer) or a thin wall zirconia rotor (provided with two spacers to ensure center packing similarly to the sapphire rotor).

Alginic acid (10 mg, alginic acid sodium salt from brown algae (medium viscosity), purchased from Merck, Cat. No. A2033) was dissolved in 0.3 mL of the D_2O solution of azobenzene (2.5 mg mL^{-1} solution, ~7 mM). Alkaline conditions (*e.g.*, from 0.025 M NaOH) were avoided to prevent azobenzene precipitation. A separate solution of $CaCl_2$ (0.018 M) in D_2O containing azobenzene was also prepared. To form the hydrogel, 0.2 mL of the $CaCl_2$ solution was added to the alginic acid solution and mixed thoroughly. This resulted in the formation of a hydrogel that was yellow in color. A 3.2 mm zirconia thin-wall rotor was packed with 34 mg of hydrogel. The sample was added to the rotor in small aliquots and compacted by spinning it down. A top spacer was placed between the sample and the cap.

4.3 Synthesis of azobenzene

The synthesis of the azobenzene and ^{13}C-methoxy azobenzene compounds and their characterization are available in the SI.

4.4 Synthesis of ethylene glycol-initiated polymers (EG-CV-10)

In a standard polymerization procedure, a 20 mL vial equipped with a magnetic stir bar was charged with ethylene glycol (EG, 0.23 g, 7.5 mmol hydroxyl groups) as the initiator. A mixture of ε-caprolactone (ε-CL) and δ-valerolactone (δ-VL) in a 1 : 1 molar ratio (ε-CL : δ-VL = 37.5 mmol : 37.5 mmol) was then introduced, followed by the addition of dried tin(II) 2-ethylhexanoate ($Sn(Oct)_2$) as the catalyst. The reaction mixture was stirred at room temperature for 10 minutes to ensure complete dissolution of all components. Subsequently, the vial was immersed in a preheated oil bath maintained at 110 °C to initiate polymerization. The conversion of monomers was monitored *via* -NMR spectroscopy by periodically withdrawing 0.1 mL aliquots from the reaction mixture. Upon reaching full conversion, the reaction vessel was removed from the oil bath and rapidly cooled using an ice bath. The resulting viscous diol-terminated polymer, designated as EG-CV-10, was obtained for further analysis.

4.5 Synthesis of lipoic acid esterified EG-CV-10 (EG-CV-10-LA)

The esterification of EG-CV-10 with lipoic acid (LA) was carried out following a previously established protocol.[65,75] Initially, EG-CV-10 (1.0 eq.) and 4-dimethylaminopyridine (DMAP, 1.4 eq.) were dissolved in 20 mL of dichloromethane (DCM) under stirring until complete dissolution was achieved. Subsequently, a separately prepared solution of α-lipoic acid (α-LA, 1.4 eq., 0.29 g) and *N*,*N*′-dicyclohexylcarbodiimide (DCC, 1.4 eq., 0.29 g) in 10 mL of DCM was added to the reaction mixture. The reaction was allowed to proceed under continuous stirring for 24 hours at room temperature.

Following the completion of the reaction, the byproduct dicyclohexylurea (DCU) was removed *via* filtration. The resulting supernatant was subjected to precipitation in cold methanol to isolate the modified polymer. To ensure the removal of residual reagents and side products, the obtained material was redissolved in DCM and reprecipitated in methanol three additional times. Finally, a final precipitation step was performed using petroleum ether. The solvent was subsequently decanted and evaporated, yielding a yellow, oil-like product.

Author contributions

A. L.: resources, investigation, formal analysis, writing – original draft; reviewing & editing; P. v. d. M.: methodology, resources; E. N.: methodology, resources; M. M. L.: resources, writing; M. R. M. G.: resources, writing; X. L: resources, writing; K. L. supervision, writing & editing; B. F.: resources, supervision; W. S.: resources, supervision. P. v. d. W. conceptualization, methodology, writing – original draft; reviewing & editing.

Conflicts of interest

There are no conflicts to declare.

Data availability

Solid-state NMR data files are available at Zenodo at **https://doi.org/10.5281/zenodo.16746422**.

Additional data supporting this article have been included as part of the SI. Supplementary information: supplementary data figures, additional experimental details, and information about chemical synthesis procedures and quality control data. See DOI: **https://doi.org/10.1039/d5ta06364g**.

Acknowledgements

We acknowledge funding support from the University of Groningen. We would like to acknowledge the valuable assistance of Ing. Marnick de Wolf from the university workshop for the support in installing the fiber in the probe. R. M. G. and W. S. acknowledge funding from the European Union's Horizon Europe research and innovation program under grant agreement no. 101046667 (EIC Pathfinder Grant SWOPT).

References

1 M. M. Lerch, M. J. Hansen, G. M. van Dam, W. Szymanski and B. L. Feringa, *Angew. Chem., Int. Ed.*, 2016, **55**, 10978–10999.
2 W. Szymanski, J. M. Beierle, H. A. V. Kistemaker, W. A. Velema and B. L. Feringa, *Chem. Rev.*, 2013, **113**, 6114–6178.
3 N. Ankenbruck, T. Courtney, Y. Naro and A. Deiters, *Angew. Chem., Int. Ed.*, 2018, **57**, 2768–2798.
4 P. Kobauri, F. J. Dekker, W. Szymanski and B. L. Feringa, *Angew. Chem., Int. Ed.*, 2023, **62**, e202300681.
5 Y. Liu, T. Wang and W. Wang, *Chem. Soc. Rev.*, 2025, **54**, 5792–5835.
6 F. Xu and B. L. Feringa, *Adv. Mater.*, 2023, **35**, 2204413.
7 H. Nie, J. L. Self, A. S. Kuenstler, R. C. Hayward and J. Read De Alaniz, *Adv. Opt. Mater.*, 2019, **7**, 1900224.
8 P. Nitschke, N. Lokesh and R. M. Gschwind, *Prog. Nucl. Magn. Reson. Spectrosc.*, 2019, **114–115**, 86–134.

9 E. Riedle, M. K. Roos, S. Thallmair, C. F. Sailer, N. Krebs, B. P. Fingerhut and R. De Vivie-Riedle, *Chem. Phys. Lett.*, 2017, **683**, 128–134.
10 T. Risse, D. Hollmann and A. Brückner, in *Catalysis*, Royal Society of Chemistry, Cambridge, 2015, vol. 27, pp. 1–32.
11 Y. Zhang, J. Kubicki and M. S. Platz, *J. Am. Chem. Soc.*, 2009, **131**, 13602–13603.
12 C. Stähler, D. R. S. Pooler, R. Costil, D. Sudan, P. Van Der Meulen, R. Toyoda and B. L. Feringa, *J. Org. Chem.*, 2024, **89**, 1–8.
13 L. Marzo, S. K. Pagire, O. Reiser and B. König, *Angew. Chem., Int. Ed.*, 2018, **57**, 10034–10072.
14 I. Ghosh, L. Marzo, A. Das, R. Shaikh and B. König, *Acc. Chem. Res.*, 2016, **49**, 1566–1577.
15 K. Zeitler, *Angew. Chem., Int. Ed.*, 2009, **48**, 9785–9789.
16 L. Buzzetti, G. E. M. Crisenza and P. Melchiorre, *Angew. Chem., Int. Ed.*, 2019, **58**, 3730–3747.
17 M. Goez, in *Annual Reports on NMR Spectroscopy*, Elsevier, 2009, vol. 66, pp. 77–147.
18 N. D. Dolinski, Z. A. Page, E. H. Discekici, D. Meis, I. Lee, G. R. Jones, R. Whitfield, X. Pan, B. G. McCarthy, S. Shanmugam, V. Kottisch, B. P. Fors, C. Boyer, G. M. Miyake, K. Matyjaszewski, D. M. Haddleton, J. R. De Alaniz, A. Anastasaki and C. J. Hawker, *J. Polym. Sci., Part A:Polym. Chem.*, 2019, **57**, 268–273.
19 N. D. Dolinski, Z. A. Page, F. Eisenreich, J. Niu, S. Hecht, J. Read de Alaniz and C. J. Hawker, *ChemPhotoChem*, 2017, **1**, 125–131.
20 E. Procházková, L. Čechová, J. Kind, Z. Janeba, C. M. Thiele and M. Dračínský, *Chem.–Eur. J.*, 2018, **24**, 492–498.
21 O. Torres, B. Procacci, M. E. Halse, R. W. Adams, D. Blazina, S. B. Duckett, B. Eguillor, R. A. Green, R. N. Perutz and D. C. Williamson, *J. Am. Chem. Soc.*, 2014, **136**, 10124–10131.
22 B. Procacci, P. M. Aguiar, M. E. Halse, R. N. Perutz and S. B. Duckett, *Chem. Sci.*, 2016, **7**, 7087–7093.
23 B. Reif, S. E. Ashbrook, L. Emsley and M. Hong, *Nat. Rev. Methods Primers*, 2021, **1**, 2.
24 A. Mandal, J. C. Boatz, T. B. Wheeler and P. C. A. van der Wel, *J. Biomol. NMR*, 2017, **67**, 165–178.
25 I. Matlahov and P. C. A. Van der Wel, *Methods*, 2018, **148**, 123–135.
26 P. Schanda and M. Ernst, *Prog. Nucl. Magn. Reson. Spectrosc.*, 2016, **96**, 1–46.
27 J. L. Uribe and R. W. Martin, *J. Magn. Reson.*, 2024, **19**, 100153.
28 J. Matysik, N. Alia, J. G. Hollander, T. Egorova-Zachernyuk, P. Gast and H. J. de Groot, *Indian J. Biochem. Biophys.*, 2000, **37**, 418–423.
29 T. M. Osborn Popp, N. H. Alaniva and A. B. Barnes, *J. Magn. Reson.*, 2021, **8–9**, 100019.
30 J. G. Hu, B. Q. Sun, M. Bizounok, M. E. Hatcher, J. C. Lansing, J. Raap, P. J. E. Verdegem, J. Lugtenburg, R. G. Griffin and J. Herzfeld, *Biochemistry*, 1998, **37**, 8088–8096.
31 M. G. Zysmilich and A. McDermott, *J. Am. Chem. Soc.*, 1994, **116**, 8362–8363.
32 A. J. Rossini, *J. Phys. Chem. Lett.*, 2018, **9**, 5150–5159.
33 A. B. Barnes, G. De Paëpe, P. C. A. van der Wel, K.-N. Hu, C.-G. Joo, V. S. Bajaj, M. L. Mak-Jurkauskas, J. R. Sirigiri, J. Herzfeld, R. J. Temkin and R. G. Griffin, *Appl. Magn. Reson.*, 2008, **34**, 237–263.
34 J. M. Griffiths, K. V. Lakshmi, A. E. Bennett, J. Raap, C. M. Van Der Wielen, J. Lugtenburg, J. Herzfeld and R. G. Griffin, *J. Am. Chem. Soc.*, 1994, **116**, 10178–10181.
35 A. Barde, R. Han, M. A. Olson, M. Tonelli, C. M. Rienstra, K. A. Henzler-Wildman and T. Ravula, *Angew. Chem., Int. Ed.*, 2025, e202501440.
36 T. J. N. Hooper, R. De Oliveira-Silva and D. Sakellariou, *J. Mater. Chem. A*, 2025, **13**, 933–939.
37 A. Naito, Y. Makino, A. Shigeta and I. Kawamura, *Biophys. Rev.*, 2019, **284**, 1–15.
38 G. J. Janssen, P. Bielytskyi, D. G. Artiukhin, J. Neugebauer, H. J. M. de Groot, J. Matysik and A. Alia, *Sci. Rep.*, 2018, **8**, 17853.
39 E. Roy, Alia, P. Gast, H. van Gorkom, H. J. M. de Groot, G. Jeschke and J. Matysik, *Biochim. Biophys. Acta, Bioenerg.*, 2007, **1767**, 610–615.
40 J. C. Zill, Z. He, M. Tank, B. H. Ferlez, D. P. Canniffe, Y. Lahav, P. Bellstedt, A. Alia, I. Schapiro, J. H. Golbeck, D. A. Bryant and J. Matysik, *Photosynth. Res.*, 2018, **137**, 295–305.
41 K. B. Sai Sankar Gupta, E. Daviso, G. Jeschke, A. Alia, M. Ernst and J. Matysik, *J. Magn. Reson.*, 2014, **246**, 9–17.
42 M. G. Zysmilich and A. E. McDermott, *Proc. Natl. Acad. Sci. U. S. A.*, 1996, **93**, 6857–6860.
43 P. Bielytskyi, D. Gräsing, S. Zahn, K. R. Mote, A. Alia, P. K. Madhu and J. Matysik, *J. Magn. Reson.*, 2019, **298**, 64–76.
44 J. C. Lansing, M. Hohwy, C. P. Jaroniec, A. F. L. Creemers, J. Lugtenburg, J. Herzfeld and R. G. Griffin, *Biochemistry*, 2002, **41**, 431–438.
45 M. L. Mak-Jurkauskas, V. S. Bajaj, M. K. Hornstein, M. Belenky, R. G. Griffin and J. Herzfeld, *Proc. Natl. Acad. Sci. U. S. A.*, 2008, **105**, 883–888.
46 J. Herzfeld and J. C. Lansing, *Annu. Rev. Biophys. Biomol. Struct.*, 2002, **31**, 73–95.
47 K. Oshima, A. Shigeta, Y. Makino, I. Kawamura, T. Okitsu, A. Wada, S. Tuzi, T. Iwasa and A. Naito, *Photochem. Photobiol. Sci.*, 2015, **14**, 1694–1702.
48 J. G. Hu, B. Q. Sun, A. T. Petkova, R. G. Griffin and J. Herzfeld, *Biochemistry*, 1997, **36**, 9316–9322.
49 A. Naito and I. Kawamura, in *Advances in Biological Solid-State NMR: Proteins and Membrane-Active Peptides*, Royal Society of Chemistry, Cambridge, 2014, pp. 387–404.
50 Y. Makino, I. Kawamura, T. Okitsu, A. Wada, N. Kamo, Y. Sudo, K. Ueda and A. Naito, *Biophys. J.*, 2018, **115**, 72–83.
51 H. Yomoda, Y. Makino, Y. Tomonaga, T. Hidaka, I. Kawamura, T. Okitsu, A. Wada, Y. Sudo and A. Naito, *Angew. Chem., Int. Ed.*, 2014, **53**, 6960–6964.
52 A. Naito, Y. Tasei and I. Kawamura, in *Experimental Approaches of NMR Spectroscopy*, Springer Singapore, Singapore, 2018, pp. 135–170.
53 J. de Mos, A. Jakob, J. Becker-Baldus, A. Heckel and C. Glaubitz, *Chem.–Eur. J.*, 2020, **26**, 6789–6792.

54 M. Doroudgar, J. Morstein, J. Becker-Baldus, D. Trauner and C. Glaubitz, *J. Am. Chem. Soc.*, 2021, **143**, 9515–9528.

55 K. L. Willett and R. A. Hites, *J. Chem. Educ.*, 2000, **77**, 900.

56 Y. Ji, D. A. DiRocco, C. M. Hong, M. K. Wismer and M. Reibarkh, *Org. Lett.*, 2018, **20**, 2156–2159.

57 F. A. Jerca, V. V. Jerca and R. Hoogenboom, *Nat. Rev. Chem.*, 2021, **6**, 51–69.

58 R. Parlato, J. Volarić, A. Lasorsa, M. Bagherpoor Helabad, P. Kobauri, G. Jain, M. S. Miettinen, B. L. Feringa, W. Szymanski and P. C. A. Van Der Wel, *J. Am. Chem. Soc.*, 2024, **146**, 2062–2071.

59 D. Topgaard, *Pure Appl. Chem.*, 2023, **95**, 1075–1089.

60 M. El Hariri El Nokab, A. Lasorsa, K. O. Sebakhy, F. Picchioni and P. C. A. van der Wel, *Food Hydrocolloids*, 2022, **127**, 107500.

61 K. Y. Lee and D. J. Mooney, *Prog. Polym. Sci.*, 2012, **37**, 106–126.

62 A. Nowacka, N. A. Bongartz, O. H. S. Ollila, T. Nylander and D. Topgaard, *J. Magn. Reson.*, 2013, **230**, 165–175.

63 L. Li, J. M. Scheiger and P. A. Levkin, *Adv. Mater.*, 2019, **31**, 1807333.

64 I. Tomatsu, A. Hashidzume and A. Harada, *Macromolecules*, 2005, **38**, 5223–5227.

65 X. Lan, L. Boetje, T. Pelras, C. Ye, F. Silvianti and K. Loos, *Polym. Chem.*, 2023, **14**, 5014–5020.

66 M. Khan, M. R. Shaik, S. T. Khan, S. F. Adil, M. Kuniyil, M. Khan, A. A. Al-Warthan, M. R. H. Siddiqui and M. Nawaz Tahir, *ACS Omega*, 2020, **5**, 1987–1996.

67 L. Schaffer, D. Preiss, R. S. Palani, N. Wiesner, J. Liu, S. Strymish, S. Bahri, S. Linse, N. Gershenfeld and R. G. Griffin, *J. Magn. Reson.*, 2025, **379**, 107909.

68 J. Matysik, Y. Ding, Y. Kim, P. Kurle, A. Yurkovskaya, K. Ivanov and A. Alia, *Appl. Magn. Reson.*, 2022, **53**, 521–537.

69 F. De Biasi, M. A. Hope, Y. Qiu, P. J. Brown, M. Visegrádi, O. Ouari, M. R. Wasielewski and L. Emsley, *J. Phys. Chem. Lett.*, 2024, **15**, 5488–5494.

70 J. Kemmink, G. W. Vuister, R. Boelens, K. Dijkstra and R. Kaptein, *J. Am. Chem. Soc.*, 1986, **108**, 5631–5633.

71 R. K. Harris, E. D. Becker, S. M. C. De Menezes, P. Granger, R. E. Hoffman and K. W. Zilm, *Magn. Reson. Chem.*, 2008, **46**, 582–598.

72 J. J. Helmus and C. P. Jaroniec, *J. Biomol. NMR*, 2013, **55**, 355–367.

73 F. Delaglio, S. Grzesiek, G. W. Vuister, G. Zhu, J. Pfeifer and A. Bax, *J. Biomol. NMR*, 1995, **6**, 277–293.

74 A. E. Bennett, C. M. Rienstra, M. Auger, K. V. Lakshmi and R. G. Griffin, *J. Chem. Phys.*, 1995, **103**, 6951–6958.

75 C. Liu, R. Lu, M. Jia, X. Xiao, Y. Chen, P. Li and S. Zhang, *Chem. Mater.*, 2023, **35**, 2588–2599.